Surface & Coatings Technology 220 (2013) 164–169

Contents lists available at SciVerse ScienceDirect

Surface & Coatings Technology

journal homepage: www.elsevier.com/locate/surfcoat

Study of impingement of hollow ZrO_2 droplets onto a substrate

Arvind Kumar [a], Sai Gu [a,*], Hani Tabbara [a], Spyros Kamnis [b,c]

[a] School of Engineering Sciences, University of Southampton, Southampton SO17 1BJ, UK
[b] PyroGenesis S.A., Technological Park of Lavrio, 19500 Lavrio, Greece
[c] Civil Engineering Department, Xi'an Jiaotong-Liverpool University, Suzhou Industrial Park, Jiangsu Province, China

ARTICLE INFO

Available online 4 September 2012

Keywords:
Thermal spray
Hollow droplet
Model

ABSTRACT

In this paper a numerical study comparing the impingement behaviour of a hollow droplet and an analogous continuous droplet onto a substrate is presented. In the impingement model the transient flow dynamics during impact, spreading and solidification of the droplet are considered. The results of droplet spreading and solidification indicate that the impact process of the hollow droplet on the substrate is distinctly different from an analogous continuous droplet. The hollow droplet results in counter liquid jetting during the impact process, larger solidification time for the splat, smaller and thicker splat as compared to the analogous continuous droplet.

© 2012 Elsevier B.V. All rights reserved.

1. Introduction

The quality of the coating in the thermal spraying process is directly affected by the droplet impingement process on the substrate in which individual splats are formed. The heat transfer between the impinging droplet and the substrate controls the rate of cooling and solidification that plays a vital role in the splat formation. Many works [1–6] are being devoted to the modelling and simulation of the droplet impact process; these works have improved the understanding of droplet deformation, spreading, solidification and adhesion with the surfaces. Validation of these models has substantiated their ability to successfully predict the droplet spreading behaviour after impact with the substrate [1,3,5] with the correct number of fingers surrounding a three dimensional splat [4]. The theoretical and experimental studies of droplet impingement [1–6], however, assume that the droplets are continuous without any voids inside. The impingement of hollow droplet onto surfaces is not well addressed and hence the current understanding of the impact behaviour of hollow particles in thermal spraying is very limited.

Hollow and porous particles can be obtained by spray dried agglomerates [7–10]. These porous powder particles during their in-flight motion in the thermal plasma jet form hollow liquid droplets prior to their impact with the surface [8,11]. The limited studies reported in this field [7,8,12] suggest that the resulting coating from hollow melt droplets opens up new prospects for improved coating characteristics (e.g., controlled coating porosity). By controlling the coating porosity thermal insulation properties of the coatings can be enhanced [12–14], which will have potential applications in turbine blade, engine component coatings. Furthermore, in spraying of hollow particles, it can be expected that the shell material in such particles undergoes complete melting, with the temperature being quite uniform across the particle [8]. Apart from influencing the droplet impact behaviour onto the substrate, the voids within the powder particles can influence the particle in-flight behaviours in the thermal spray coating process such as, particle acceleration, melting and oxidation [9].

In this article we study the impact process of a hollow droplet onto a flat surface. The results for hollow droplet spreading, solidification and formation of splat are compared with those of an analogous conventional continuous droplet.

2. Numerical simulation

We consider the problem of the impact of a single spherical hollow ZrO_2 droplet such that immediately prior to droplet–surface collision, the droplet consists of a liquid shell enclosing a gas (air) cavity. A molten ZrO_2 hollow spherical droplet at an initial uniform temperature of 2970 K (outer diameter $D_0 = 50$ μm and void diameter $d_0 = 25$ μm) impinges with a velocity U_0 (100 m/s) onto a flat substrate kept at an initial temperature of 300 K. Table 1 shows the material properties data [15,16]. A two-dimensional axisymmetric formulation (Fig. 1), based on a previously validated model of a continuous dense droplet [3], is considered. In the impingement model transient flow dynamics during impact, spreading and solidification are considered using the volume of fluid surface tracking method (VOF) coupled with a solidification model within a one-domain continuum approach based on the classical mixture theory [3,17]. The governing conservation equations are given in Table 2.

2.1. Free surface modelling

The VOF model is used to track the interface between the droplet and the air considering these two as immiscible fluids by solving a

* Corresponding author. Tel.: +44 23 80 596506; fax: +44 23 80 593058.
E-mail address: s.gu@soton.ac.uk (S. Gu).

0257-8972/$ – see front matter © 2012 Elsevier B.V. All rights reserved.
http://dx.doi.org/10.1016/j.surfcoat.2012.08.061

Table 1
Material properties data.

Impinging droplet material	Zirconia (ZrO_2)
Substrate material	Stainless steel (SS)
Gas phase (the void and the droplet surrounding medium)	Air (air)
Droplet initial temperature	2970 K
Substrate initial temperature	652 K
Solidus temperature (ZrO_2) [16]	2949 K
Liquidus temperature (ZrO_2) [16]	2951 K
Thermal conductivity (liquid ZrO_2) [16]	$2.00\ W \cdot m^{-1}/K$
Thermal conductivity (solid ZrO_2) [16]	$2.32\ W \cdot m^{-1}/K$
Thermal conductivity (SS)	$14.9\ W \cdot m^{-1}/K$
Thermal conductivity (air)	$0.0242\ W \cdot m^{-1}/K$
Density (liquid ZrO_2)	$5700\ kg/m^3$
Density (solid ZrO_2) [16]	$5890\ kg/m^3$
Density (SS)	$7900\ kg/m^3$
Density (air)	$1.225\ kg/m^3$
Droplet surface tension [15]	0.43 N/m
Contact angle [15]	90°
Viscosity (liquid ZrO_2) [15]	$0.021\ kg \cdot m^{-1}/s$
Viscosity (air)	$1.7894 \times 10^{-5}\ kg \cdot m^{-1}/s$
Specific heat capacity (solid and liquid ZrO_2) [15]	$713\ J \cdot kg^{-1}/K$
Specific heat capacity (SS)	$477\ J \cdot kg^{-1}/K$
Specific heat capacity (air)	$1006.43\ J \cdot kg^{-1}/K^1$
Latent heat of fusion [16]	$7.07 \times 10^5 J/kg$

single set of momentum equations. This method tracks the volume fraction of each of the fluids throughout the computational domain. Accordingly, the governing equations are being solved in both air and molten droplet domains. The volume of fraction of fluid in a control volume (F) has a range of zero to unity; the cells having F values between zero and one represent the air–molten droplet interface, $F=0$ indicates that the cell contains only air, and $F=1$ corresponds to a cell full of droplet material. The volume of fraction function F is advected using the continuum mixture velocity field as given by the VOF equation (Eq. (1)).

2.2. Momentum and heat transport modelling

As we consider different densities of the solid and the liquid phases, f_l and g_l will be different and they are related by the relation given in Eq. (2). The value of f_l is evaluated from the local temperature based on the solution of the energy conservation Eq. (6). In the present model shrinkage will take place because of different solid and liquid phase densities and the flow due to the contraction is compensated by air. The pressure outlet boundary condition considered at the outer part of the computational domain will facilitate this. For computational cells which are undergoing phase change, the solid–liquid interaction in the momentum conservation Eq. (4) is evaluated using Darcy's model of viscous flow through a porous medium [3,17] using the source term Su. This term is active only for cells filled with molten droplet and vanishes at the free surface and in the air phase. The parameter C in this term is a constant (assumed 150,000 [3]) that accounts for the solidification phase morphology. The continuum surface tension force F_{vol} in Eq. (4) is calculated by the method described in [18]. The momentum and the energy conservation equations are coupled. The source term S_h appearing in the energy conservation Eq. (6) is active only for the computational cells filled with molten droplet ($F=1$). In the substrate only the conduction heat transfer is solved (Eq. (9)). For the substrate thermal contact resistance a constant value of $1.8 \times 10^{-6}\ m^2\ K\ W^{-1}$, corresponding to a stainless steel substrate roughness of 0.06 μm, is used [3]. The field of hollow droplet impact is new, and thermal contact resistance of hollow droplets are not well known, therefore, to begin with we used the same thermal contact resistance for the continuous and the hollow droplets. This enables us to clearly distinguish the influence of other parameters in the simulations.

The initial conditions for the physical system are: at $t=0$, droplet temperature (void and shell) $T_d=2970$ K, $F=1$ in the droplet shell, $F=0$ in the droplet void; droplet impact velocity = 100 m/s (vertically downward); $u=v=F=0$, $T_{air}=300$ K in the air domain, $T_{subs}=300$ K. The void in the hollow droplet is of the same gas (i.e., air) which surrounds the droplet. The thermal boundary condition at the side and bottom of the substrate is a fixed temperature of 300 K, and other boundary conditions for the problem are shown in Fig. 1.

3. Results and discussion

3.1. Impact behaviour

The dynamic impingement process of the hollow droplet is shown in Fig. 2. The result for the spreading of an analogous continuous droplet (same mass) is also displayed. During the impact process the hollow droplet undergoes deformation of the droplet shell and of the void within the droplet (0.2 μs), stretching of the void cavity and thinning of the droplet shell (0.4 μs) followed by rupture of the shell (0.8 μs). At the *first stage* of the impact process the lower hemispherical shell comes into contact with the substrate surface, and progressively deforms and spreads along the substrate. At the same time, the upper hemispherical shell proceeds with the motion with initial velocity. At the *second stage* stretching of the void cavity and thinning of the droplet shell take place. At the *third stage* rupture occurs at the periphery of the upper hemisphere. Between *first* and *third stages* a central counter jet of liquid forms which moves upward (0.4 μs onwards). This counter liquid jetting phenomenon captured is similar to that observed in the experimental

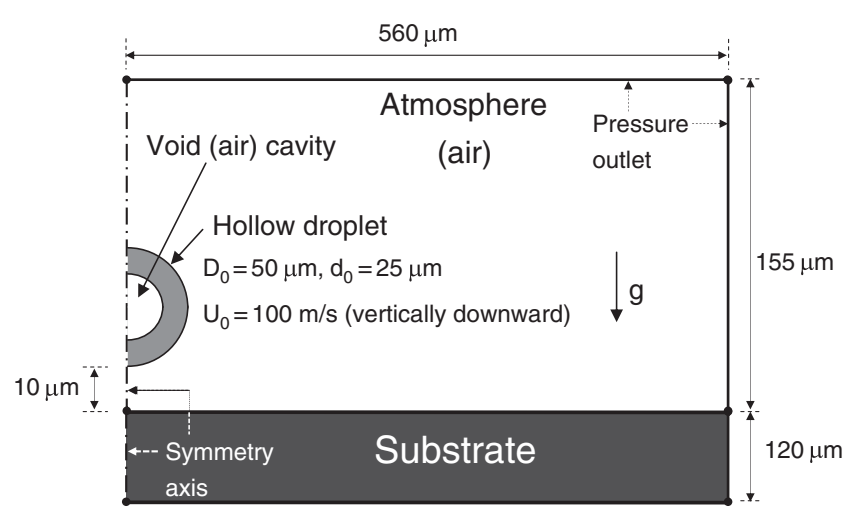

Fig. 1. Schematic diagram of the axisymmetric computational domain.

Table 2
Governing conservation equations.

VOF equation:

$$\frac{\partial F}{\partial t} + \nabla \cdot \vec{u} F = 0$$

Mixture quantities definitions for a cell in the mushy state:

$$g_l + g_s = 1, \quad f_l + f_s = 1, \quad f_l = \frac{g_l \rho_l}{\rho_d}, \quad \rho_d = g_l \rho_l + (1-g_l)\rho_s$$
$$\rho = F\rho_d + (1-F)\rho_{air}, \quad c_{eff} = Fc_d + (1-F)c_{air}$$
$$k_{eff} = Fk_d + (1-F)k_{air} \quad \text{with } k_d = g_l k_l + (1-g_l)k_s, \quad \mu = F\mu_d + (1-F)\mu_{air}$$

Continuity:

$$\frac{\partial}{\partial t}(\rho) + \nabla \cdot \left(\rho \vec{u}\right) = 0$$

Momentum conservation;

$$\frac{\partial}{\partial t}\left(\rho \vec{u}\right) + \nabla\left(\rho \vec{u}\, \vec{u}\right) = -\nabla p + \nabla\left[\mu\left(\nabla \vec{u} + \nabla \vec{u}^T\right)\right] + \rho \vec{g} + F_{vol} - \mu_{air}$$

$$S\vec{u} = \left\{ \left[C\frac{(1-g_l)^2}{g_l^3}\right] \vec{u}\, F = 10 F < 1 \right.$$

Energy conservation:

$$\frac{\partial}{\partial t}\left(\rho c_{eff} T\right) + \nabla \cdot \left(\rho \vec{u} c_{eff} T\right) = \nabla \cdot \left(k_{eff} \nabla T\right) + S_h$$

$$S_h = \begin{cases} -L\left[\frac{\partial}{\partial t}(\rho f_l) + \nabla \cdot \left(\rho \vec{u} f_l\right)\right] & F = 1 \\ 0 & F < 1 \end{cases}$$

$$f_l = 0 \quad \text{if} \quad T \le T_{solidus}$$
$$f_l = 1 \quad \text{if} \quad iT \ge T_{liquidus}$$
$$f_l = \frac{T - T_{solidus}}{T - T_{liquidus}} \quad \text{if} \quad iT_{solidus} < T < T_{liquidus}$$

Substrate heat transfer:

$$\frac{\partial}{\partial t}\left(\rho_{subs} c_{subs}{}^{subs} T\right) = \nabla \cdot (k_{subs} \nabla T)$$

where,

c	Specific heat capacity
C	Constant related to Darcy source term
D_0	Initial droplet diameter
d_0	Initial void diameter
f_l	Weight fraction of liquid
f_s	Weight fraction of solid
F	Volume of fluid function
F_{vol}	Continuum surface tension force
$\vec{g}$	Acceleration due to gravity vector
g_l	Volume fraction of liquid
g_s	Volume fraction of solid
k	Thermal conductivity
L	Latent heat of fusion
T	Time
T	Temperature
U_0	Initial droplet impact velocity
$\vec{u}$	Continuum velocity vector
Greek symbols	
M	Dynamic viscosity
P	Density
Subscript	
D	Droplet
Subs	Substrate
Air	Air
Eff	Effective
L	Liquid
0	Initial
s	Solid

[11] and numerical [19] studies reporting on the impact of a hollow droplet of glycerin. The upward moving counter liquid jet finally breaks off from the lower part (10 μs) and keeps moving in an upward direction. In our simulations with a high-velocity droplet impact (100 m/s), the velocity of the counter jet is also high (~20–30 m/s). We believe that the breaking off phenomenon is due to high velocity in the upward moving counter jet. Subsequently the detached part starts to fall upon the splat (20 μs) and finally solidifies (35 μs). In our simulations the volume of the upward jet is about 12% of the initial droplet volume. From this about half of the counter jet breaks off and accordingly the disintegrated mass is overall 6% of the initial droplet mass. The present case that does not consider any mass loss of the detached volume can then predict the upper limit of the deposition efficiency. This will be useful for the optimisation of the hollow droplet thermal spray coating process. The droplet reaches its maximum spread at 3 μs (this will be shown in Fig. 5). After this surface tension pulls the edges of the droplet inwards and the spreading stabilizes from 25 μs when the droplet mainly solidifies.

The impact sequence of an analogous continuous droplet is shown in the right side of Fig. 2. Based on a spherical shape for the droplet the

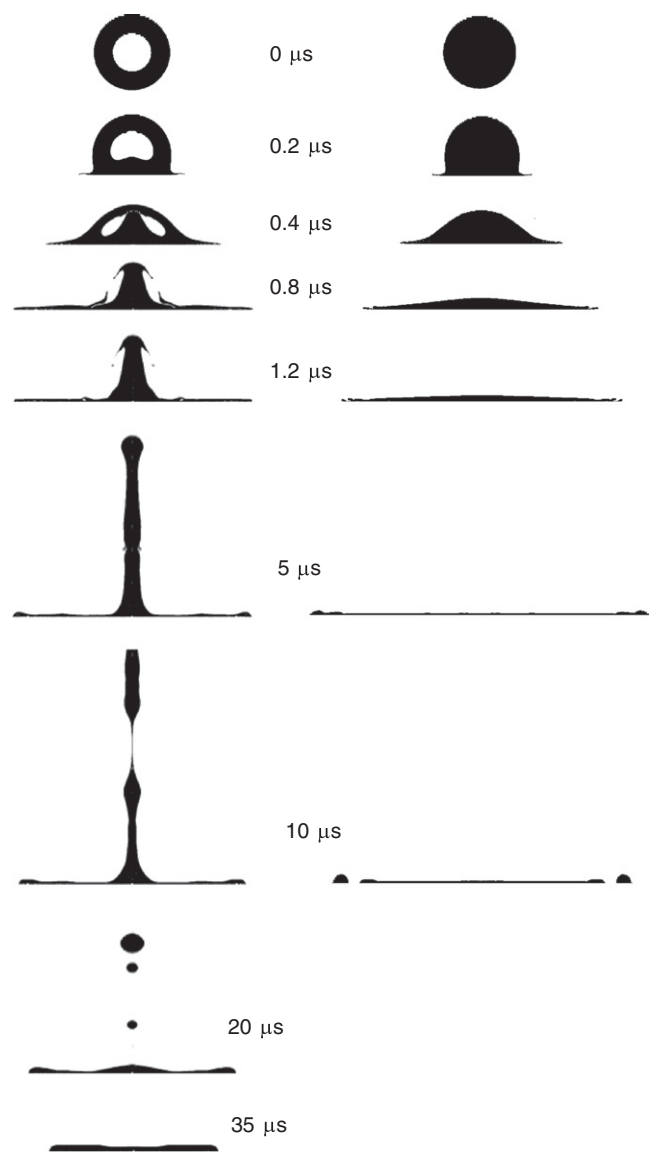

Fig. 2. Snapshots of droplet spreading on the substrate for hollow (left) and analogous continuous (right) droplet.

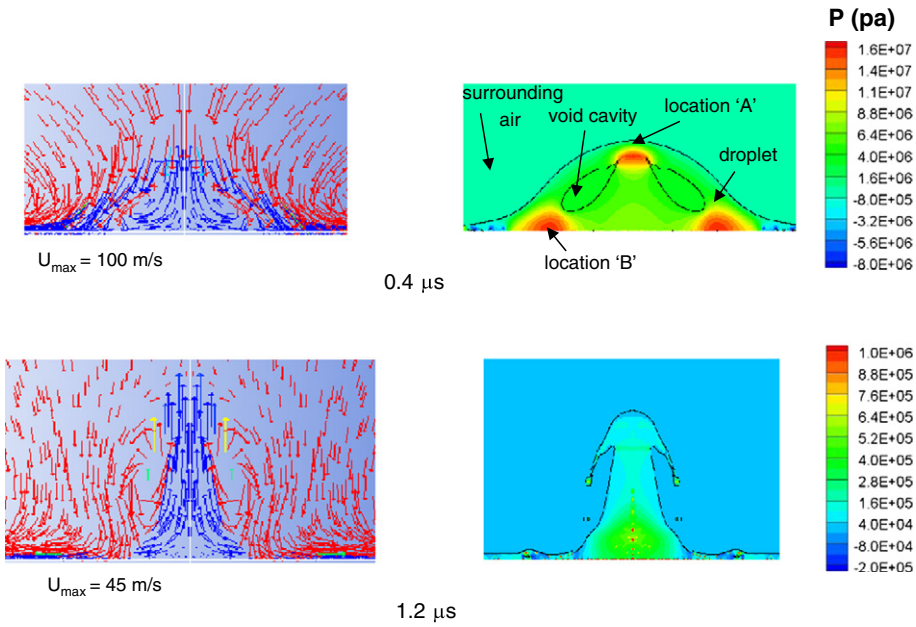

Fig. 3. Velocity (left) and gauge pressure (right) distribution in the hollow droplet. The red colour velocity vectors are in the air (surrounding and void cavity) and the blue colour vectors are in the droplet. The pressure maps (right) also show the superimposed contour of the droplet fraction = 1.

diameter of the analogous continuous droplet (same mass as that of the hollow droplet) is $0.956 \cdot D_0$. The other impact conditions are the same as that of the hollow droplet. The continuous dense droplet spreads radially along the substrate surface after impact. It was noticed that the droplet reaches its maximum spread at 3 μs which will be shown subsequently in Fig. 5. After this surface tension pulls the edges of the droplet inwards and the spreading stabilizes from 9 μs when the droplet mainly solidifies. A detailed discussion of this typical spreading behaviour for a continuous droplet can be found in [1–5] and hence this discussion is not repeated here. From this result the distinct impact behaviour for the case of the hollow droplet can be noticed, specifically, the phenomenon of counter jetting, a smaller and thicker final splat. The continuous dense droplet causes break-up in the splat. On the other hand, hollow droplet results in a continuous splat. In this way the hollow droplet forms a more uniform splat than the continuous droplet. The term 'uniform splat' is mentioned in the sense when there is no break-up in the splat and the thickness of the splat is quite uniform.

In order to understand the formation of central counter jetting the velocity and the pressure distributions in the hollow droplet are shown in Fig. 3. At 0.4 μs the internal pressure in the void portion of the hollow droplet is estimated to be three times lower than that in the dense droplet. This low pressure in the internal region of the hollow droplet, due to lack of the impinging mass, generates a steep pressure gradient from the periphery to the centre of the droplet. This causes the flow of liquid from the periphery to the centre, creating a counter jet. We can see that at 0.4 μs when the droplet shell is about to rupture, the flow from the upper hemispherical shell (location 'A') follows the spreading path. However, there is also a backward vortex from the shell–surface contact location 'B' towards the centre of the droplet. This backward flow is caused by a pressure build up at location 'B' (at 0.4 μs). At a subsequent time the pressure build up location shifts towards the centre of the droplet (at 1.2 μs) and the backward vortex generated earlier creates an upward flow at the centre of the droplet. From the shell–substrate contact location 'B' a part of the liquid flows towards the centre, that generates a radially converging liquid stream. This creates the central counter jet. Liquid is continuously supplied to the counter jet from the shell, and the thickness of the shell continuously decreases which finally ruptures (at 0.8 μs). Meanwhile, the radial converging flow in the central counter jet that is directed along the outer normal to the substrate creates an upward movement of the counter jet. It was estimated that the maximum values of the flow velocity in the spreading path along the substrate and in the counter jet are respectively 75 m/s and 20 m/s at 0.4 μs, and 25 m/s and 25 m/s at 1.2 μs. The flow velocity in the counter jet stabilizes after this time. The flow velocity in the spreading path decreases sharply with time, which slows down the droplet spreading along the substrate.

3.2. Solidification behaviour

The snapshots of droplet solidification for the hollow and the analogous continuous droplet are shown in Fig. 4. For the continuous droplet a thin solidification layer is developed at the substrate surface at 0.4 μs. The solidification layer increases in size (height and diameter) as the droplet spreads (0.8 μs). The solidification at the edge causes the start of the break up in the spreading droplet material at the edge. This creates a break up in the splat (1.2 μs). After this the flow due to surface tension at the edges pulls the edges of the droplet inwards which decreases the diameter of the splat [1–5]. The droplet solidifies fully at 10 μs having a discontinuous splat (i.e., break up in the splat). For the hollow droplet a similar behaviour of the solidifying zone is observed except for the fact that the part of the droplet in fully liquid state is relatively much larger because of the upward motion of the counter liquid jet and its breaking off from the bottom splat. This causes the detached part to remain not in contact with the bottom splat for a long time. This reduces the heat extraction from the detached part, and accordingly the final solidification time for the hollow droplet is much larger (35 μs) than the continuous droplet (10 μs). As we noticed earlier for the hollow droplet the flow velocity in the spreading path along the substrate decreases sharply with time (from 75 m/s to 25 m/s between 0.4 μs and 1.2 μs). However, for the continuous dense droplet between these times the decrease in the flow velocity in the spreading path along the substrate is not that large (from 75 m/s to 45 m/s), which in turn, leads to a faster spreading with the continuous droplet. This along with solidification at the edge in the case of the continuous droplet causes break up in the spreading droplet material, and finally forms a discontinuous splat (break up in the splat).

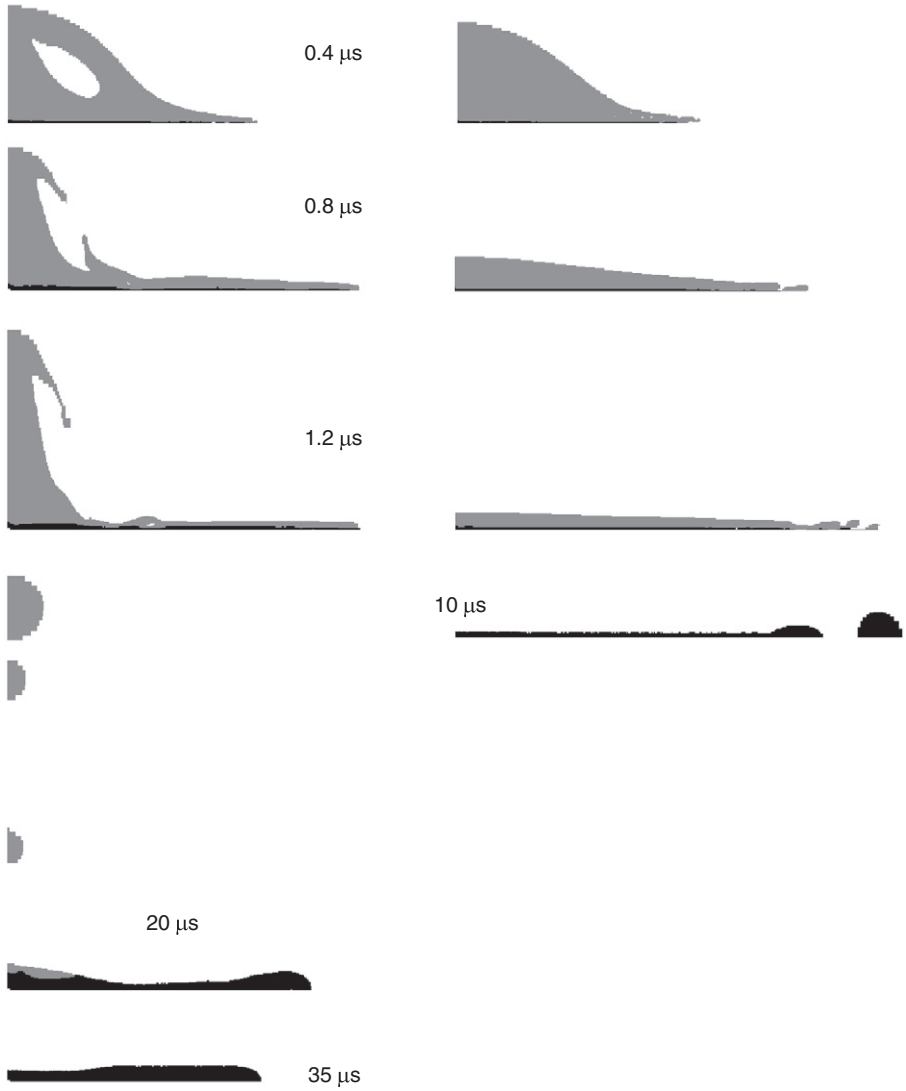

Fig. 4. Snapshots of droplet solidification for hollow (left) and analogous continuous droplets (right). Only the axisymmetric half of the droplet is shown. The black colour shows the zone with a liquid fraction lower than one (mushy or fully solid) and the grey colour shows a fully liquid zone. The boundary of the grey colour is the droplet–air interface.

In the present case of high impact velocity the initial impact and splashing is controlled by the inertia of the hollow droplet. We estimated that in our simulations the flattening splashing in the dense droplet was due to solidification. For other cases, for example for lower impact velocity, the splashing could also be caused by inherent instability of a thin liquid film and/or by the interaction with the surrounding air [6]. In the simulations the substrate is at room temperature, which can enhance the solidification at the edge and cause break up in the splat [20]. Substrates at some preheated temperature can suppress this break up in the splat [20]. In the case of the hollow droplet slower spreading along the substrate is observed which does not cause any break up in the spreading droplet material. Further, a large central counter liquid jet forms with the hollow droplet which slowly falls and moves smoothly with a much lower velocity upon a solidified splat (20 μs). These factors lead to a smaller and continuous final splat in the case of the hollow droplet.

Fig. 5 displays a quantitative comparison of the transient spread factor for the hollow and the analogous continuous droplet. The spread factor is defined as the ratio of the instantaneous splat diameter to the initial droplet diameter. It can be noticed that the hollow droplet results in a much smaller splat diameter compared to the continuous droplet (45% smaller). Previously also, it was experimentally demonstrated that the dimensionless diameter of the ZrO_2 splat, under otherwise equivalent conditions, is significantly smaller for a hollow particle than for the dense one [8].

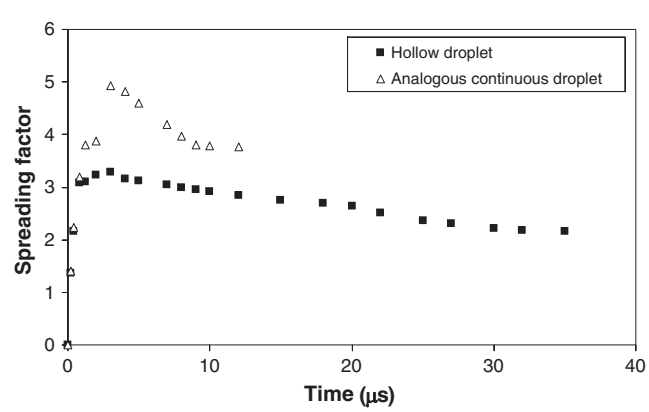

Fig. 5. Transient variation of droplet spreading factor.

4. Conclusion

The hollow droplet shows some distinct features compared to the analogous continuous droplet during the impact, its subsequent spreading and formation of the splat on the substrate. The void in the droplet causes a phenomenon of counter liquid jetting during the impact process, similar to that reported in the experiment [11]. The hollow droplet results in a large central splash, a smaller final splat diameter, a thicker and more uniform splat as compared to the analogous continuous droplet. The solidification time for the splat formed with hollow droplet is also relatively large. In our results, in contrast to a continuous droplet, a hollow droplet does not cause any break up in the spreading droplet material and forms a continuous splat. This work, demonstrating our first results for the behaviour of the hollow droplet impact, is a starting step to understand the less known behaviour of hollow particles in thermal spray coating formation. In future work we will address the influence of substrate characteristics such as, roughness, wetting, and droplet characteristics such as, velocity, temperature on the impact behaviour and subsequent splat formation with the hollow droplets.

Acknowledgement

The financial support from the EC FP7 Simuspray project (Grant No. 230715) is gratefully acknowledged.

References

[1] S.D. Aziz, S. Chandra, Int. J. Heat Mass Transfer 43 (2000) 2841.
[2] S. Shakeri, S. Chandra, Int. J. Heat Mass Transfer 45 (2002) 4561.
[3] S. Kamnis, S. Gu, J. Phys. D: Appl. Phys. 38 (2005) 3664.
[4] S. Kamnis, S. Gu, T.J. Lu, C. Chen, J. Phys. D: Appl. Phys. 41 (2008) 165303 (7 pp.).
[5] S. Chandra, P. Fauchais, J. Therm. Spray Technol. 18 (2009) 148.
[6] H. Tabbara, S. Gu, Int. J. Heat Mass Transfer 55 (2012) 2081.
[7] O.P. Solonenko, A.V. Smirnov, and I.P. Gulyaev, in AIP Conference Proceedings, ed. by M. Tokuyama, I. Oppenheim and H. Nishiyama, Vol. 982, 2008, p. 561
[8] O.P. Solonenko, I.P. Gulyaev, A.V. Smirnov, Tech. Phys. Lett. 34 (2008) 1050.
[9] S. Kamnis, S. Gu, M. Vardavoulias, J. Therm. Spray Technol. 20 (2011) 630.
[10] J. Kovacik, J. Mater. Sci. Lett. 18 (1999) 1007.
[11] I.P. Gulyaev, O.P. Solonenko, P.Yu. Gulyaev, A.V. Smirnov, Tech. Phys. Lett. 35 (2009) 885.
[12] K. Shinoda, H. Murakami, J. Therm. Spray Technol. 19 (2010) 602.
[13] M.P. Planche, S. Costil, C. Verdy, C. Coddet, Appl. Phys. A: Mater. Sci. Process. 99 (2010) 665.
[14] F. Rousseau, C. Fourmond, F. Prima, M.H. Vidal Serif, O. Lavigne, D. Morvan, P. Chereau, Surf. Coat. Technol. 206 (2011) 1621.
[15] K. Shinoda, M. Raessi, J. Mostaghimi, T. Yoshida, H. Murakami, J. Therm. Spray Technol. 18 (2009) 609.
[16] H. Tabbara, S. Gu, Appl. Phys. A: Mater. Sci. Process. 104 (2011) 1011.
[17] N. Pathak, A. Kumar, A. Yadav, P. Dutta, Appl. Therm. Eng. 29 (2009) 3669.
[18] J.U. Brackbill, D.B. Kothe, C. Zemach, J. Comput. Phys. 100 (1992) 335.
[19] A. Kumar, S. Gu, S. Kamnis, Appl. Phys. A: Mater. Sci. Process. (2012), http://dx.doi.org/10.1007/s00339-012-7043-y.
[20] K. Alamara, S. Saber-Samandari, P.R. Stoddart, C.C. Berndt, Surf. Coat. Technol. 206 (2011) 1180.